Mon. Not. R. Astron. Soc. **360,** 227–235 (2005) doi:10.1111/j.1365-2966.2005.09029.x

The effects of clumping on derived abundances in H II regions

John S. Mathis[1]★ and Kenneth Wood[2]★

[1]*Astronomy Department, University of Wisconsin, 475 N. Charter Street, Madison, WI 53706, USA*
[2]*School of Physics and Astronomy, University of St Andrews, North Haugh, St Andrews, Fife KY16 9SS*

Accepted 2005 March 18. Received 2005 March 16; in original form 2004 December 1

ABSTRACT

We have compared Monte Carlo photoionization models of H II regions with a uniform density distribution with models with the same central stars and chemical compositions but with a three-dimensional hierarchical density distribution consisting of clumps within clumps, on a four-tier scheme. The purpose is to compare the abundances of He, N, O, Ne and S obtained by standard analyses (emission-line strengths and measured mean temperatures from [O III] and [N II]) with the abundances in our models. We consider stellar temperatures in the range 37.5–45 kK and ionizing photon luminosities from 10^{48} to 10^{51} s^{-1}.

Clumped models have different ionic abundances than uniform. For hot stars, (He^0/H^+) is 2–3 per cent, much larger than with uniform models. This amount of He^0 is independent of metallicity and so impacts the determination of the primordial abundance of He. The total abundances of O, Ne and S obtained by the usual methods of analysis, using T([O III]) for high stages of ionization and T([N II]) for low, are about as accurate for clumped models as for uniform, and within ∼20 per cent of the true values. If T([O III]) is used for analysing all ions, the derived (O/H) is ∼40–60 per cent too large for cool stars but is good for hot stars. Uniform models have similar errors, so the clumping does not change the accuracy of abundance analysis.

The physical causes of the ionic abundance errors are present in real nebulae. In clumped models, helium ionizing radiation from zones of high ionization (low He^0 and low ultraviolet opacity) can penetrate nearby regions near the edge of the ionized zone. This effect allows He^0 to absorb more stellar photons than in uniform or radially symmetrical geometries. In turn, these absorptions compete with O^+, etc., for those energetic stellar photons.

Key words: radiative transfer – ISM: general – H II regions – cosmology: miscellaneous.

1 INTRODUCTION

The interstellar medium (ISM) has filamentary structure over scales ranging from hundreds of parsec through astronomical units. In this paper, we analyse some of the properties of H II regions formed by ionization of the clumpy interstellar gas and we compare them to those produced by the same code for models with a spatially uniform density. The Monte Carlo photoionization code (Wood, Mathis & Ercolano 2004) treats gas with densities that have a power-law or scale-independent character over about an order of magnitude in spatial sizes (see Section 2). We refer to these hierarchical models as 'clumped'.

Our goal is to isolate the effects of clumping by comparing clumped models with smooth density distributions, while keeping other important parameters (e.g. the stellar atmospheres and luminosities that strongly influence the nebular models, and the nebular composition) constant. We choose the other parameters rather arbitrarily and do not try to compare our models with real objects. Several types of questions motivate us, as follows.

(i) For a fixed exciting star and mean nebular density, how are the ionization and temperature structures of the resulting ionized nebulae affected? What are the physical causes of the differences? How do the differences vary as the nebular parameters (e.g. the exciting star properties, the geometry of the clumps and the mean gas density) are changed?

(ii) How accurately are model ionic abundances determined from the emission lines, using techniques similar to those commonly used to analyse observations of real nebulae? What errors occur in the ionic abundances derived from ratios of fluxes of emission lines, using mean nebular electron temperatures, T_e, estimated from diagnostic line ratios?

We assume idealized conditions, neglecting observational errors and reddening of emission lines by interstellar dust either within or exterior to the H II region. Thus, our abundance errors are lower

★E-mail: mathis@astro.wisc.edu (JSM); kw25@st-andrews.ac.uk (KW)

limits to those expected for real nebulae. We consider the effects of dust in the transfer of Lyman continuum radiation within the ionized gas.

Our assumptions and the limits of parameter space that we have explored are given in Section 2. In Section 3 we consider the physical differences among the clumped models and their differences from uniform models. In Section 4, we discuss the relevance of our models to real nebulae and the uncertainties of abundances within them.

We do not address the important issue of differences in abundances of many ions derived from recombination lines as opposed to collisionally excited lines. A common explanation is that there are 'anomalous' temperature variations within the ionized plasma (see, for example, García-Rojas et al. 2004, and references therein), although the phenomenon seems more complicated (e.g. Tsamis et al. 2003). We have used only standard physics, and our abundances from recombination lines would be almost the same as from collisionally excited lines.

2 ASSUMPTIONS USED IN THE MODELS

There are many free parameters that affect the spectrum and abundances derived from model H II regions, and we consider only a subset of possible parameter space. We make the following assumptions.

(i) The models are in a steady state, thereby neglecting the dynamics occurring near the outer $H^+ \rightarrow H^0$ ionization front, where probably a D-type front (see, for example, Osterbrock 1989) is propagating into the surrounding neutral material. This is the standard assumption in H II region models. However, the conditions near the ionization front are important for N^0 and O^0, which are sensitive to the temperature and ionization structure at the outer edge of the ionized region.

(ii) We chose the composition used for workshops for testing model H II regions (Ferland 1995; Péquignot et al. 2001): H, He, C, N, O, Ne and S = 1, 0.1, 2.2×10^{-4}, 4.0×10^{-5}, 3.3×10^{-4}, 9.0×10^{-6} and 5.0×10^{-5}, respectively, by number. These abundances are rather arbitrary, but are adequate for investigating the important physical effects introduced by clumping. We refer to elemental abundances as chemical symbols without superscripts, so that (O/H) is the abundance ratio of O, including all stages of ionization, relative to H.

(iii) Dust in H II regions and within the diffuse ionized gas (DIG) needs careful consideration. We show below that carbonaceous grain material has probably largely been converted to the gas phase. We find that the effects of carbon-depleted dust are not very significant, but that with other assumptions dust could become dominant in determining the structure of the ionized region.

Dust affects the emitted nebular spectrum by reddening the nebular radiation and also by absorbing ionizing radiation. Because corrections for reddening are routinely made, we assume that line strengths are determined perfectly. This assumption is very optimistic when we consider the spatially unresolved emission-line fluxes rather than the pixel-by-pixel line intensities (see Section 3.2).

If there were no destruction of dust within the ionized zone, the absorption of ionizing radiation by dust would be hugely important, while dust scattering, strongly directed forward, has almost no effect. The absorption cross-section of graphitic carbon, closely related to absorption by polycylic aromatic hydrocarbons (PAHs), peaks at about 17 eV with a cross-section of 3×10^{-21} cm^2 (H atom)$^{-1}$ according to the model of Weingartner & Draine (2001), with the cross-sections conveniently tabulated by B. T. Draine (see http://www.astro.princeton.edu/∼draine). This exceeds the opacity of H if $(H^0/H) \leqslant 0.001$, which occurs over most of the volume of the nebula. Dust with this carbonaceous cross-sections absorbs ∼90 per cent of the ionizing radiation over our entire range of models, for all geometries. By contrast, the silicate component of dust is relatively grey in the ionizing ultraviolet, with an opacity of roughly 1.3×10^{-22} cm^2 H^{-1}, only 5 per cent of the peak of carbonaceous dust.

The abundance of dust in H II regions can be estimated by means of the gas-phase abundances of refractory elements (e.g. C, Al, Mg, Ca or Fe; see Savage & Sembach 1996) that are mostly locked up in dust in the diffuse ISM. Abundances found in bright H II regions are significantly different, especially for C. In the diffuse neutral ISM, the C II abundances derived from absorption towards 12 B stars is C/H = 160 ± 17 ppM and an upper limit of 108 ppM for another (Sofia et al. 2004). In various H II regions, gas phase C/H varies from 330 to 590 ppM (Esteban et al. 1999a,b, 2004; García-Rojas et al. 2004). Solar (C/H) = 245 ± 30 ppM (Asplund et al. 2005; Holweger 2001). Interstellar abundances have probably been significantly enhanced since the formation of the Sun, perhaps dex(0.2) to ∼400 ppM (e.g. Pagel & Tautvaišienė 1995; Ackerman et al. 2004). The Orion Bar (Sellgren et al. 1990), an ionization front seen edge-on, shows 3.3-μm aromatic hydrocarbon emission arising from a rather thin zone between the Pα and Brα recombination lines of H and emission lines of H_2. Thus, several observations require that bright H II regions have most or almost all of their carbon in the gas phase. Usually H II regions have strong near-infrared emission bands, but it may be that the carriers are actually in the neutral gas adjacent to the ionized.

In some H II regions, silicaceous dust is present within the ionized gas. In M17, only about 15 per cent of the Fe is in the gas phase (Esteban et al. 1999b). Within the DIG, Howk & Savage (1999) found that Al III/S III is much less than solar. Both ions are found only in the gas in which H is ionized, so Al is depleted on to grains in the DIG. Further direct evidence for dust within the DIG is given by the correlation of the diffuse Hα with 100-μm emission and the lack of correlation with H I (Lagache et al. 2000).

In summary, it seems that the carbonaceous component of dust has largely been vaporized in H II regions while the silicaceous grains may largely remain intact. Perhaps processes that convert carbon in grains to the gas phase act very rapidly in ionized gas, so that the C in dust (including PAHs and the 'very small grains', carbonaceous in character) does not absorb ionizing radiation when H is mostly H^+. Pure silicate dust has cross-sections so low and so weakly dependent on wavelength that its presence is not crucial to the results of this paper. We ran models that confirmed this statement, but for most models in this paper we neglected dust and also heating by PAHs.

(iv) Our algorithm for clumping was not derived from any model of turbulence, but rather from hierarchically clumped models of the density distributions in the manner described in Mathis, Whitney & Wood (2002), following Elmegreen (1997). Points were placed within a cube as described below. The cube was partitioned into 65^3 cells, and the final gas density within each of the cells was proportional to the number of points falling within the cell. The exciting star was placed at the centre of the cube. Initially, 32 points were cast randomly throughout the cube. Surrounding each of these, another 32 points were cast randomly within a distance determined by the 'fractal dimension', D, of the model (see Mathis et al. 2002 for details). Around each of these points, another 32 were nested, and finally 32 more around each of the preceding rounds of casting. Thus, the structure, if it were continued indefinitely, would be considered 'fractal', but the power spectrum is a power law only over about a

decade in sizes of projected densities. The mean density was taken to be $n(\mathrm{H}) = 100$ cm^{-3}, with a fraction f_{smooth} in a uniform distribution and the rest in the clumped cells. f_{smooth} represents an average over a still finer distribution of subclumps, not spatially resolved in our simulation, which extend down to very small scales.

For this paper we chose $f_{\mathrm{smooth}} = 0.15$, so the minimum density of a cell is 15 cm^{-3}. The maximum density within these models was 2700 cm^{-3}, with a spread of ± 15 per cent arising from different initial seeds. For comparison with the clumped geometries, uniform models were computed with the same stellar luminosity and $n(\mathrm{H}) = 100$ cm^{-3}. The uniform models fitted more compactly into the grid cube, and consequently could employ a mesh 2.7 times finer than the clumped models. The abundance patterns found with the coarse and finer resolution uniform models are in close agreement except for O^0 (the coarse being 1.5–2.2 times larger).

In order to test the effects of allowing radiation to escape from our clumped models through vacuum instead of unresolved cells, we ran models with $f_{\mathrm{smooth}} = 0$. About 10 per cent of the ionizing photons escaped the simulation, as opposed to $\sim$1.5 per cent for the $f_{\mathrm{smooth}} = 0.15$ models.

The distribution of the density in the clumped models is determined by three parameters: f_{smooth}, the initial seed for the random number generator and the 'fractal dimension', D, which determines the power spectrum of column densities as projected from an assumed cube on to the plane of the sky. We have considered $D = 2.6$ and 2.9, and averaged all clumped models among the same five arbitrarily chosen initial seeds. Thus, we have an indication of the dispersion of various physical quantities among clumpy models with the same fractal dimension.

(v) The H-ionizing photon luminosity of the exciting star in units of 10^{49} photons s^{-1}, L_{49}, was increased from 0.1 to 100, in steps of factors of 10. For uniform models, this is equivalent to changing the 'ionization parameter', $U \equiv 10^{49}\, L_{49}/(4\pi R_{\mathrm{S}}^2\, n_{\mathrm{e}} c)$, by factors of $10^{1/3}$ (R_{S} is the Strömgren radius and n_{e} is the electron density.) A large U implies large abundances of high stages of ionization and a relatively sharp increase of $(\mathrm{H}^0/\mathrm{H})$ near the edge of the Strömgren sphere. In clumped models, the ionized region is not spherical and there is no constant value of n_{e}, but L_{49} is an equivalent parameter to explore the effects represented by U in uniform models. For instance, our results are applicable to superstar clusters: $L_{49} \sim 10^3$–10^4, $n_{\mathrm{e}} \sim 10^3$–10^4 cm^{-3} in starburst galaxies.

(vi) The dielectronic recombination coefficients for sulfur are poorly known. Unfortunately, they can be important for the ionization of S. We followed Ali et al. (1991), using averages of various ions of C, N and O. We tested the importance of these assumptions by calculating some models with all dielectronic recombinations for S being zero. Of course, this is an extreme assumption, because a lack of knowledge of the values of coefficients does not imply that they are zero. We discuss the results in Section 3.5.4

The cube for clumped models was large enough so that $\lesssim$1 per cent of the ionizing radiation escaped through the edges. The outer boundaries of the ionized regions were very irregular in shape, and for all stellar temperatures there are a few regions of neutral H and He embedded within the ionized gas, with the gas that they shadow from the star ionized by recombination radiation.

(vii) Our cell sizes are large in comparison with the mean free paths of ionizing photons when H is almost neutral within the cell. Our code derives a mean ionization for the cell based on the radiation entering it without considering any substructure of the ionization within the cell. Our analysis attributes that ionization to the entire mass of the cell, while only a fraction of the cell's mass would actually be involved. Near the edge, a few photons can produce ionizations that the code assumes are spread uniformly over the entire cell, with a correspondingly low electron density. Therefore, recombinations are underestimated, and too much mass of ionized material is derived. The principal ions for which this effect occurs are H^0, N^0 and O^0. In our analysis we considered only cells in which the code derived $(\mathrm{H}^0/\mathrm{H})$ less than $\mathrm{H}^0_{\mathrm{min}}$, a parameter taken to be 0.25 for the results in this paper. This choice provides roughly an optical depth of unity across our cells, for a typical photon that can reach the edge. We have investigated how these results depend on $\mathrm{H}^0_{\mathrm{min}}$. Uniform models are hardly affected because the area of their almost-neutral H zone is much smaller than clumped models. These show a slow decline in $(\mathrm{He}^+/\mathrm{H}^+)$ as $\mathrm{H}^0_{\mathrm{min}}$ is increased from 0.1 to 0.4, and a more rapid drop from 0.4 to 0.9. The increase of $n(\mathrm{H}^0)/n(\mathrm{H})$ between adjacent cells is typically an order of magnitude when the larger $(\mathrm{H}^0/\mathrm{H})$ is 0.4 or more.

We kept the number of cells within the model cube constant and varied the physical length of the cube proportional to $L_{49}^{1/3}$. This makes clumped models with the same initial seed have the same ionization structure in terms of the size of the model cube.

Fig. 1 shows the clumped gas densities in a typical slice through the plane containing the star (upper left), the fraction of H^0 in the same slice (upper right), the intensities of Hα, relative to its maximum intensity, as projected on to the sky (with no foreground extinction; lower left), and the [N II]/Hα ratio projected on to the sky (lower right). The axes are in parsec for a model with $T^* = 40$ kK, $L_{49} = 10$. We see that the density through the midplane is

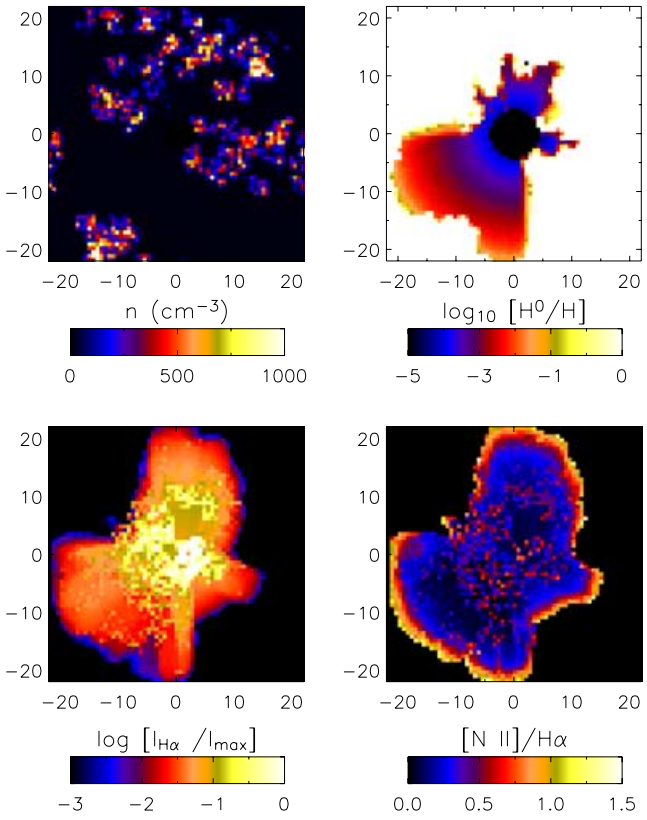

Figure 1. Some properties of the models for $L_{49} = 10$, $T^* = 40$ kK. The axes give distances in pc. Upper left: a slice through the midplane (containing the star), showing the densities in the models. Upper right: the fraction of neutral H. Lower left: a projection of the Hα intensity upon the plane of the sky, normalized to the maximum intensity. Lower right: the projected [N II]6583/Hα ratios.

concentrated to the left side, but the projected images (lower left and lower right) are more symmetrical because of ionization in the foreground and background planes. [N II]/Hα is large at the edge because the ionization favours N^+ and the temperature is relatively high there.

The large [N II]/Hα (Fig. 1, lower right) at the edges does not imply that the H II region would appear limb-brightened in the sky. The lower left panel shows that the Hα intensity at the edges is only $\sim$1 per cent as bright as the maximum, so the [N II] intensity is low and would blend in with the unrelated surrounding diffuse emission. It is only the [N II]/Hα ratio that increases at the edges.

3 EFFECTS OF CLUMPING ON IONIC ABUNDANCES

Our results from a large number of models can be summarized simply. For a given exciting star, clumping changes the averaged fraction of ionization of all elements, but differently for relatively cool stars than for hot. The important quantity is $\gamma \equiv (L_{\rm He}/L_{\rm H})/({\rm He/H})$. If $\gamma > 1$, a star is 'hot'; <1, 'cool'. Clumping enhances the higher stages of ionization of an element (including He) for cool stars and decreases them for hot. The amounts of enhancement for specific ions are discussed below.

We have $L_{\rm He} = \int L^*_\nu/h\nu \, {\rm d}\nu$, integrated from the ionization potential of He^0, $\chi(He^0) = 24.6$ eV to $\chi(He^+) = 54$ eV. $L_{\rm H}$ is $\int L^*_\nu/h\nu \, {\rm d}\nu$, integrated from 13.6 to 54 eV. We count the radiation above 24.6 eV as both H- and He-ionizing because each recombination of He produces about one H-ionizing photon (Osterbrock 1989), so absorptions by He hardly affect the number of H-ionizing photons. Interstellar dust does not affect the distribution of ionization significantly if it contains only silicates, as seems likely (see Section 2).

3.1 Influences of parameters

There are a large number of parameters in our models. Some set the basic physics and radiative transfer (elemental abundances, T^*, L_{49} and $f_{\rm smooth}$) but others are arbitrary (the fractal dimension, D, and the initial seed that determines the density structure in clumped models). The dispersion of the results among the five initial seeds that we arbitrarily chose for each clumped model is not large. Typical variations of (H^+/H) are 0.1 per cent; of (He^0/He), 0.2 per cent if $(He^0/He) \leqslant 0.1$ and <2 per cent if $(He^0/He) \sim 0.3$. The mean temperatures weighted by $n_{\rm e}\, n(H^+)$ vary $\sim$0.5 per cent. Varying D from 2.6 to 2.9 produced changes about twice the dispersion among the various seeds of each clumped model. The overall result is that the other parameters were much more influential than D and the initial seed. For the rest of the paper, we present $D = 2.6$ results as representing clumped models, with results averaged among the five seeds.

We begin by considering the main physical difference between clumped and uniform models, then we define averaged abundances for comparing models, and then we consider specific elements and ions.

3.2 Propagation of He-ionizing radiation

The most important consequence of a clumped density distribution is the fate of He-ionizing radiation, depending upon the hardness of the stellar radiation. It determines the relative amounts of the nebular opacity supplied by H and He, the two big players for almost all ionizing photons.

Hot stars produce bountiful He-ionizing photons, so H can compete with He for He-ionizing radiation. At $h\nu = 25$ eV, just above $\chi(He^0)$, H contributes $\sim$40 per cent of the opacity near the star with $T^* = 45$ kK, and He practically all of the rest. In a uniform model, the fraction of H opacity gradually falls with distance from the star as He becomes more neutral. In the interclump regions of clumped models, the H opacity decreases less rapidly with distance because the density is lower. The abrupt increase of density when stellar photons encounter a clump makes the increase of He opacity over H occur within a small volume. The overall effect is to make H compete for He-ionizing radiation more effectively in clumped models than in smooth, thereby decreasing (He^+/He) and other high stages of ionization over uniform models.

He supplies 95 per cent of the opacity for 25-eV photons when $T^* = 37.5$ kK. In this case, in clumped models the He is ionized in the interclump medium until the outflowing starlight encounters a clump, at which point both H and He tend to become neutral. In a uniform model, the He goes neutral after it absorbs essentially all of the stellar He-ionizing radiation, and there is a substantial region in which H is still H^+ but He is neutral. The overall effect is that He and H tend to be both ionized within the same volume in clumped models, so the (He^+/He) within the ionized region is larger than in uniform models. The same effect applies to other high stages of ionization. This is the major physical cause of differences between clumpy and smooth models.

We have compared clumped models with those with uniform densities, but the root physical causes of the differences lie in the radial symmetry, not the uniformity, of the uniform models. The general distinctions between clumped and uniform models applies to any smooth distribution of gas density.

We considered Kurucz (1994) stellar atmospheres of (37.5, 40, 42.5 and 45) kK, $\log g = 4$ and we used a power-law interpolation between them to estimate spectra for 38.1, 38.7 and 41 kK as well. For these atmospheres, $\gamma = 1$ occurs at about 39.1 kK. We will see qualitative differences in the ionization structure for other elements at this T^*. For Kurucz atmospheres, $\gamma = (0.569, 1.35, 2.41)$ for $T^* = (37.5, 40, 45)$ kK. We present plots of ionization fractions versus T^* because γ, the real independent variable, is a less familiar quantity.

3.3 Comparing models with observables

Our aim is to compare the abundances within our clumped models with the abundances that would be inferred if the emissions from the models, measured without error or dust, were interpreted in the ways used on actual nebulae. The derived abundances differ from the actual ones in the model because of temperature and density variations within the model, even if the density is never enough to de-excite the emission lines by collisions. If there is poor spatial resolution, there is averaging over the face of the nebula as well. We compare three types of averaged abundances of a particular ion, X^i, relative to H. The line emission (photons cm^{-3} s^{-1} sr^{-1}) is $n(X^I) n_{\rm e}\, j_\lambda(X^i, T_{\rm e})$, and j_λ is presumed to be known from atomic theory.

Because the model provides three-dimensional ionization structure of the nebula, the true abundances are known:

$$\left(\frac{X^i}{H^+}\right)_{\rm true} = \frac{\int n(X^i)\, {\rm d}V}{\int n(H^+)\, {\rm d}V}. \quad (1)$$

An observer would know the projected line intensities, $I_\lambda = \int n(X^i) n_{\rm e}\, j_\lambda(X^i, T_{\rm e})\, {\rm d}z$, where z is the distance along the line of sight, averaged over the observer's spatial resolution. An extreme

assumption would be that there is no spatial resolution over the face of the nebula, so that we know only the total line fluxes, F_λ, thereby obtaining a 'global' averaged abundance:

$$F_\lambda = \int I_\lambda \, \mathrm{d}x \, \mathrm{d}y, \tag{2}$$

$$= \int n(\mathrm{X}^i) n_\mathrm{e} \, j_\lambda(\mathrm{X}^i, T) \, \mathrm{d}V. \tag{3}$$

$$\left(\frac{\mathrm{X}^i}{\mathrm{H}^+}\right)_\mathrm{global} = \frac{F_\lambda(\mathrm{X}^i)/j_\lambda(\mathrm{X}^i, T_\mathrm{X})}{F(\mathrm{H})/j_\mathrm{H}(T_\mathrm{H})} \tag{4}$$

$$= \frac{\int n(\mathrm{X}^i)\, w(\mathrm{X}^i)\, \mathrm{d}V}{\int n(\mathrm{H}^+)\, w(\mathrm{H})\, \mathrm{d}V}, \tag{5}$$

where T_X is the measured averaged temperature relevant to the ion X^i, depending upon whether it is a high or low stage. The weights $w(\mathrm{X}^i) = n_\mathrm{e}\, j_\lambda(\mathrm{X}^i, T)$, and similarly for the H lines. For high ions, we use T([O III]), obtained from [O III]λ4363/(5007+4859). For low ions, we use T([N II]), from [N II]λ5755/(6583+6548).

We explore the effects of the $w(\mathrm{X}^i)$ on the derived abundances. Note that the effect is not limited to variations in temperature: it exists even in artificial isothermal models because of variations in n_e.

Another extreme assumption is that $(\mathrm{X}^i/\mathrm{H})$ can be determined at each point (x, y), and the result, $A_\mathrm{X}(x, y)$, then averaged, weighting the bright pixels more than the faint. We define the abundances averaged over the face of the nebula by

$$\left(\frac{\mathrm{X}^i}{\mathrm{H}^+}\right)_\mathrm{ave} = \frac{\int A_\mathrm{X}(x, y)\, I_\mathrm{H}(x, y)\, \mathrm{d}x\, \mathrm{d}y}{\int I_\mathrm{H}(x, y)\, \mathrm{d}x\, \mathrm{d}y}. \tag{6}$$

The fluctuations of temperature within our models are modest, as uniform and smooth models have previously suggested. The variation of T([O III]) across the face of a nebula (e.g. O'Dell, Peimbert & Peimbert 2003) is described by $t^2 = \int (T(x, y) - T_0)^2 \mathrm{d}x\, \mathrm{d}y / [T_0^2 \int \mathrm{d}x\, \mathrm{d}y]$, where $\mathrm{d}x\, \mathrm{d}y$ is the element of area on the sky and T_0 is the averaged temperature. O'Dell et al. (2003) found t^2 in the range 0.005–0.016 in five regions of the face of the Orion nebula using *Hubble Space Telescope* images of λ4363 and 5007 with high spatial resolution. For $T^* = 40$ kK and $L_{49} = 10$, our models collapsed along one axis yielding $t^2 = 0.0012$ for the uniform model and (1.0–1.6) × 10^{-3} for the clumped models with various initial seeds. For $T^* = 45$ kK, $t^2 \sim 0.002$. Thus, the Orion nebula shows temperature fluctuations in excess of models, but not enough to explain the discrepancies between collisionally excited and recombination lines, unless one assumes that in real nebulae more violent fluctuations are averaged out by the integration along the line of sight.

We do not discuss fine structure lines ([O III] 52, 88 μm, plus several others) because their emissivities are not sensitive to variations in temperature or densities within the rather modest ranges that we consider. These lines provide excellent diagnostics of the true abundances of their respective ions for both clumped and uniform models, but are subject to collisional de-excitations in real objects.

We now discuss individual ions and elemental abundances.

3.4 $\mathrm{He}^+/\mathrm{H}^+$

Fig. 2 displays $(\mathrm{He}^+/\mathrm{H}^+)$ plotted against T^* for clumped models (upper sets of curves) and $(\mathrm{He}^+/\mathrm{H}^+ - 0.1)$ for uniform density distributions (lower sets of curves). The horizontal lines at $(\mathrm{He}^+/\mathrm{H}^+) =$ 0.1 and 0.09 show the cases of complete ionization of He. The solid lines are true abundances (equation 1) for $L_{49} = 0.1$; the dashed lines are for $L_{49} = 100$. The dot-dashed lines are the global abundances (which would be deduced by observers using the fluxes of lines) for $L_{49} = 0.1$; the dotted for $L_{49} = 100$. The other values of L_{49} have curves lying between those shown. The bends in the curves near $T^* = 39.5$ kK occur because $\gamma \sim 1$, so that the ratio of stellar ionizing photon luminosities for He and H, $L_\mathrm{He}/L_\mathrm{H}$ equals the elemental abundance ratio (He/H).

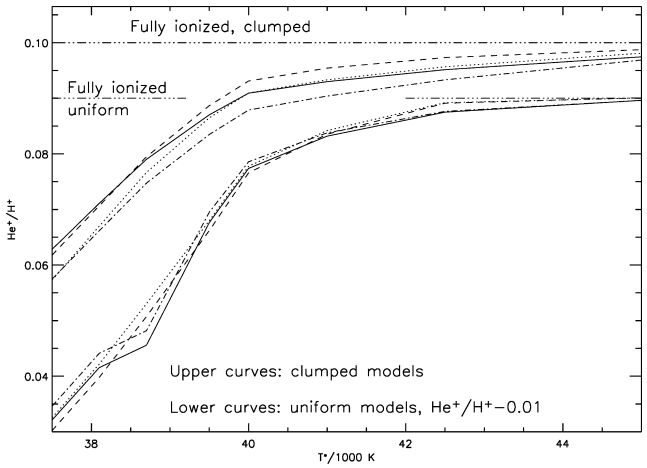

Figure 2. The ratio $(\mathrm{He}^+/\mathrm{H}^+)$ as determined for clumped (upper set of curves) and uniform models, plotted against the exciting star temperature, T^*. The uniform models show $[(\mathrm{He}^+/\mathrm{H}^+) - 0.01]$. The horizontal lines show complete ionization of He for clumped and uniform models. Solid line are true abundances (see equation 1) for stars with $L_{49} = 10^{-49} L_* = 0.1$; L_* is the ionizing photon luminosity. Dashed lines represent true abundances for $L_{49} = 100$. Dot-dashed lines are global clumped abundances that would be derived by observers (see equation 5) for $L_{49} = 0.1$. Dotted lines denote global abundances for $L_{49} = 100$. The ratio of stellar ionizing photon luminosities for He and H, $L_\mathrm{He}/L_\mathrm{H}$, equals the elemental abundance ratio (He/H) at $T^* = 39.5$ kK, producing the bends in the curves.

Fig. 2 shows that clumped models provide a larger $\mathrm{He}^+/\mathrm{H}^+$ at a given low T^* than uniform models; ∼0.06 at $T^* = 37.5$ kK, as opposed to ∼0.04 for uniform. For hot stars, the uniform models (lower set of curves) have $(\mathrm{He}^+/\mathrm{H}^+) = (\mathrm{He/H})$ to high accuracy, but this is not so for clumped nebulae. They have ∼2.5 per cent of He^0 even for $T^* = 45$ kK for the true abundances, and the derived global $(\mathrm{He}^+/\mathrm{H}^+)$ (i.e. weighted by n_e) is 98.1 per cent of (He/H). The difference between the derived $(\mathrm{He}^+/\mathrm{H}^+)$ and (He/H) is 3.8 per cent for 42.5 kK stars. The error increases for lower stellar temperatures and L_{49}.

The relatively large fraction of neutral He for clumpy nebulae surrounding hot stars has important consequences, as follows.

(i) (He/H) is a major prediction of big bang nucleosynthesis, and the comparison with real nebulae requires very high accuracy in the correction for He^0 (see Olive & Skillman 2004, for a review showing the accuracy required). The reason why clumped models exhibit more He^0 than uniform models is independent of metallicity. The observations and interpretation of He I emission lines in metal-poor extragalactic H II regions strive for accuracies of ∼1 per cent in $\mathrm{He}^+/\mathrm{H}^+$ (e.g. Peimbert, Peimbert & Ruiz 2000). There must be corrections for stellar absorption lines underlying the nebular emissions as well as density and temperature effects on the He I line strengths. Uniform or smooth models for nebulae ionized by collections of very hot stars predict that $\mathrm{He}^+/\mathrm{H}^+ = \mathrm{He/H}$. Clumped

models suggest an increase of He/H of the order of ∼3 per cent to correct for He^0. Equation (11) of Olive & Skillman (2004) suggests that uncertainties in the determination of the primordial He^+/H^+ amount to ∼10 per cent, but the correction for He^0 is systematically upwards.

(ii) Helium is dominant in determining the opacity for energetic photons that produce ions of other elements, exceeding hydrogen by a factor of a few near its ionization edge. For harder radiation ($h\nu > \chi(O^+) = 35$ eV), its main competitor, O^+, typically provides <30 per cent of the opacity, and the other ions contribute significantly less because of their relatively low elemental abundances. Thus, the increased He^0 decreases the abundances of high stages of ionization of heavy elements.

3.5 Heavy elements

For heavy elements, the ionic abundances are strongly influenced by whether He recombinations to the ground term, $h\nu \sim 25$–26 eV, can ionize the stage in question [e.g. $\chi(S^+) = 23.3$ eV], so that the He recombination radiation competes with stellar radiation. If the He radiation cannot produce ionization, for cool stars the lower stage (O^+, Ne^+, N^+) is reduced in clumped models as compared to uniform. This behaviour is similar to He^0 (Fig. 2) because lower He^0 implies a smaller opacity for hard stellar photons.

There are systematics in the temperatures measured in various ways. For all geometries, T([O III]) is cooler than the n_e-averaged temperature, $\langle T\rangle \equiv \int T\, n_e\, dV / \int n_e\, dV$, by ∼300 K because O^{+2} is a powerful coolant. T([N II]) is warmer than $\langle T\rangle$ by ∼400 K because stellar photons are always harder on average at the outer regions of the ionized gas where [N II] is produced, and O^+ is not as efficient a coolant as O^{+2}. Clumped models have warmer $\langle T\rangle$ than uniform; for $T^* = 37.5$ kK, the difference is 50–100 K; for $T^* = 45$ kK, it is ∼180 K. T([N II]) for uniform models is about 50 K larger than for clumped. These temperature differences affect the derived abundances.

3.5.1 High stages of ionization: O^{+2} and Ne^{+2}

This section deals with two ions with very similar behaviour as regards differences between uniform and clumped models: O^{+2} and Ne^{+2}. Their important characteristics are that they cannot be ionized by He recombination radiation and cannot be ionized to still higher stages by stellar radiation [$\chi(O^{+2}) = 54.9$ eV; $\chi(Ne^{+2}) = 63.4$ eV]. This group does not include S^{+2}($\chi = 34.8$ eV) because it can be ionized to S^{+3} by stellar radiation. We assume that there are only observations of N^+ optical lines and we discuss nitrogen in the next section, although there are fine-structure transitions of N^{+2} at 57 μm and of N^{+3} at 69 μm.

Fig. 3 shows (O^{+2}/O) plotted against T^* for both true abundances and the global averages, for $L_{49} = 10$. Heavy lines are clumped models and thin lines are uniform. The true abundances are solid lines and the global abundances using T([O III]) are dashed.

Fig. 4, showing (Ne^{+2}/Ne), is analogous to Fig. 3. The similarities in the ionizations are clear. Ne^{+2} starts lower than O^{+2} at low T^* but increases faster because it requires harder radiation: $\chi(Ne^+) = 40.96$ eV; $\chi(O^+) = 35.1$ eV.

Figs 3 and 4 show the following.

(i) For clumped models, the accuracy of the global (O^{+2}/O) abundances derived from T([O III]) is only ∼70–80 per cent of the true. Even perfectly accurate [O III] and Hβ line intensities do not lead to an accurate determination of O^{+2} abundances. The reason is that there are relatively strong temperature fluctuations within the O^{+2} zone in clumped models. Excess [O III] λ4363 is produced by the warmer regions, making the mean T([O III]) within the zone higher than the true mean temperature. This situation leads to an erroneously low abundance being determined for O^{+2}. (Ne^{+2}/Ne) is somewhat more accurately determined than (O^{+2}/O).

For uniform models, T([O III]) global abundances are in excellent agreement with the true. Surprisingly, the accuracy of T([O III]) abundances is better for Ne^{+2} than for O^{+2}.

(ii) The averaged spatially resolved abundances (dotted lines) are almost the same as those obtained with no spatial resolution.

(iii) The true (O^{+2}/O) and (Ne^{+2}/Ne) are larger for clumped models than for uniform in cool stars and smaller for hot stars, as was true for (He^+/H^+) (see Fig. 2).

The behaviour of (O^{+2}/O) and (Ne^{+2}/Ne) at other values of L_{49} is as expected. Decreasing L_{49} decreases high stages of ionization: for $L_{49} = 0.1$, the set of curves has the same form as those already plotted but lies entirely under the envelope of the curves shown.

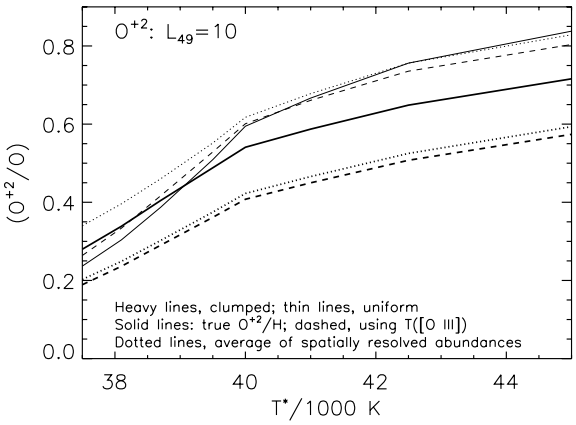

Figure 3. The fraction of oxygen in O^{+2} versus T^* for L_{49}, the exciting stellar photon luminosity in units of 10^{49} s^{-1}, = 10. The heavy lines are clumped models; the thin lines, uniform. The solid lines are the true abundances; the dashed lines are derived from T([O III]); the dotted lines are the spatially resolved abundances, averaged over the face of the nebula (see equation 6.)

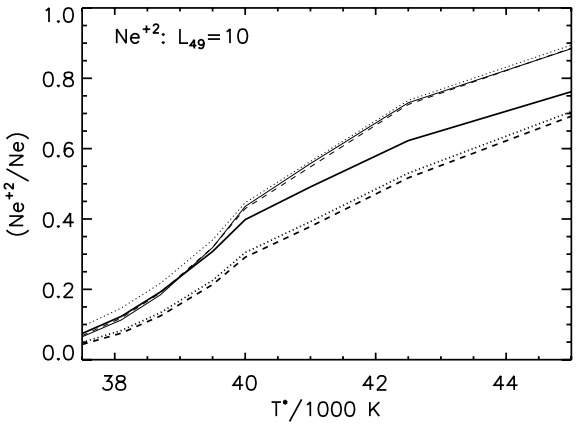

Figure 4. Plots of the (Ne^{+2}/Ne) ratio, with the same notation as used for Fig. 3. Note the strong similarities, for reasons discussed in the text.

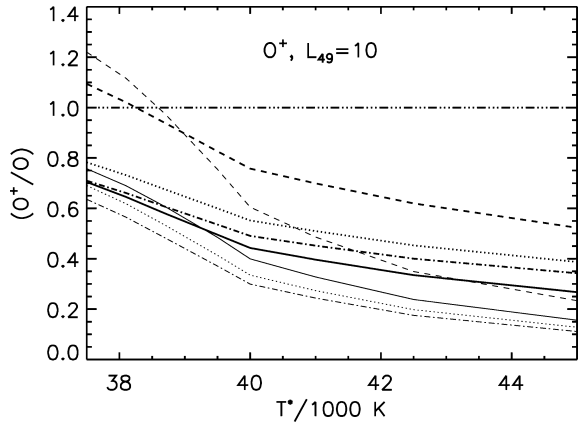

Figure 5. Global (O^+/O) versus T^* for $L_{49} = 10$. The heavy lines are clumped models; the thin, uniform. The dashed lines are derived from T([O III]); the dot-dashed lines from T([N II]). The dotted lines are averaged abundances.

3.5.2 Low stages of ionization: O^+ and N^+

These ions and their next higher stages have far larger abundances than the remaining stages of ionization (O^0, N^0 and N^{+3}) over the bulk of the nebula. Both O^+ and N^+ are further ionized only by stellar radiation: $\chi(O^+) = 35.12$ eV and $\chi(N^+) = 29.6$ eV, well above the energy of almost all He recombinations.

The (O^+/O) global ratios for $L_{49} = 10$ are shown in Fig. 5. Heavy lines are clumped models, thin lines are uniform. Solid lines are true abundances, dashed lines are global abundances derived from T([O III]) and dot-dashed lines are from T([N II]). The dotted lines are averaged abundances. Fig. 6 gives (N^+/N). Both figures show that the use of T([O III]) for a low stage of ionization is problematic, especially for cool stars. T([N II]) abundances for N^+ are ∼40 per cent too large but are, surprisingly, more accurate for (O^+/O) than for (N^+/N).

Using T([O III]) for O^+ and N^+ is especially problematic for clumped nebulae with hot exciting stars; the abundances will likely be overestimated by a factor of ∼1.5. Using T([N II]) provides results within ∼20 per cent of the true for (O^+/O) and ∼30 per cent for (N^+/N).

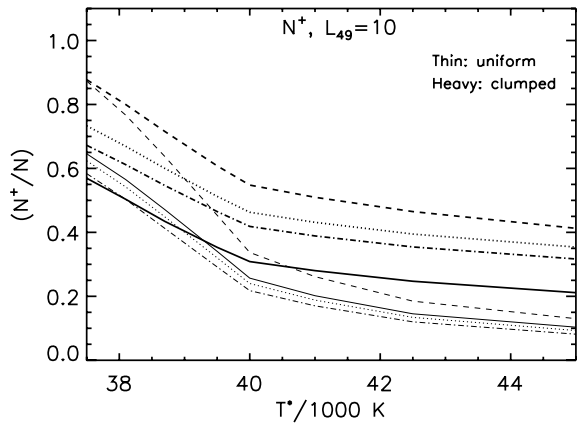

Figure 6. Plots of the N^+ against T^* for $L_{49} = 10$ for clumped models (heavy lines) and uniform models (thin lines). Solid lines are true abundances, dot-dashed lines are global abundances derived from T([N II]), dashed lines are global abundances using T([O III]) and dotted lines are average abundances (see equation 6).

3.5.3 Neutrals: O^0 and N^0

In regions where these ions are abundant, their ratio to the singly-charged species is almost completely determined by charge exchange with H^0. [O I] λ6300 emission is produced almost entirely in a physically thin zone at the outer edge of the H^+ zone. In this region there is appreciable H^0 (≳0.5 per cent) for charge exchange and a reasonably high T_e, needed to produce the collisional excitation of [O I]. Newly ionized gas flows away from the neutral material, and gas dynamics, neglected in our models, plays an important role in the local temperature and ionization structure. Both the width of the zone affected by dynamics and the mean free path of ionizing photons are less than our cell size, so we resolve this region poorly. We do not present predictions for (O^0/O), which we find to be ∼3 per cent for $L_{49} = 0.1$ and 1 per cent for $L_{49} = 100$. These values are almost surely overestimates. Our (N^0/N) is similarly unreliable. The cells in which $0.25 \leqslant (H^+/H) \leqslant 0.9$ have a mass of ∼8 per cent of the highly ionized plasma in uniform models and ∼30 per cent in clumped. However, the temperature in the partially ionized gas is falling rapidly as H^+/H decreases, so the emissions from the almost neutral gas are small. The region $0.9 < (H^+)/\,H < 0.99$ adds only ∼1 per cent to the mass and is quite cool (<6000 K), so it contributes a negligible amount of emission.

3.5.4 Sulfur

Sulfur has four relevant stages of ionization: S^+ ($\chi = 23.3$ eV, so it is ionized by the most energetic He recombination radiation); S^{+2}(χ = 34.8 eV, similar to O^{+2}); S^{+3}($\chi = 47.3$ eV); and S^{+4}. There is too little stellar radiation to make S^{+4} important in any of our models.

Figs 7 and 8 show (S^+/S) and (S^{+2}/S) plotted against T^*, both for $L_{49} = 10$. The scheme of the lines is the same as in Figs 3–6. These ions do not have the properties of the corresponding stages of oxygen (Figs 3 and 5).

Comparison of Fig. 7 with Fig. 5 reveals that S^+ has a much smaller true fractional abundance than O^+ because He recombinations ionize S^+. (S^+/S) varies far less with T^* as well. A greater fraction of O is in O^+ than S in S^+, so the clumpy nature of clumped models makes more difference for S^+. The abundance of S^+ in clumped models is three or more times larger than for uniform.

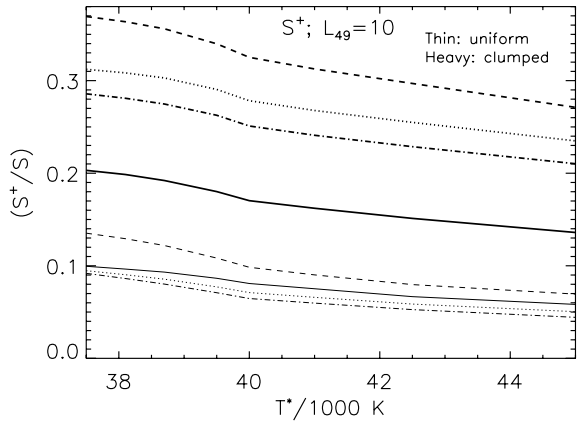

Figure 7. Plots of (S^+/S) against T^* for $L_{49} = 10$ for clumped models (heavy lines) and uniform models (thin lines). Solid lines are true abundances; dot-dashed lines, global abundances derived from T([N II]); dashed lines, global abundances using T([O III]); dotted lines, average abundances (see equation 6). Compared with Fig. 5, the same diagram for O^+, we see the influence of the ionization of S^+ by He recombination radiation that does not affect O^+.

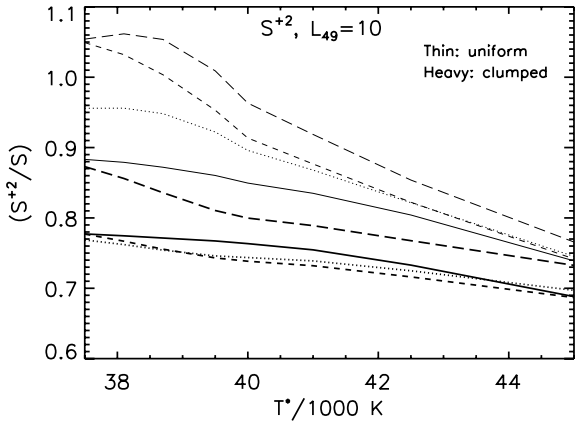

Figure 8. Plots of (S^{+2}/S) against T^* for $L_{49} = 10$ for clumped models (heavy lines) and uniform models (thin lines). Solid lines are true abundances; dashed lines, global abundances using T([O III]); dotted lines, average abundances (see equation 6).

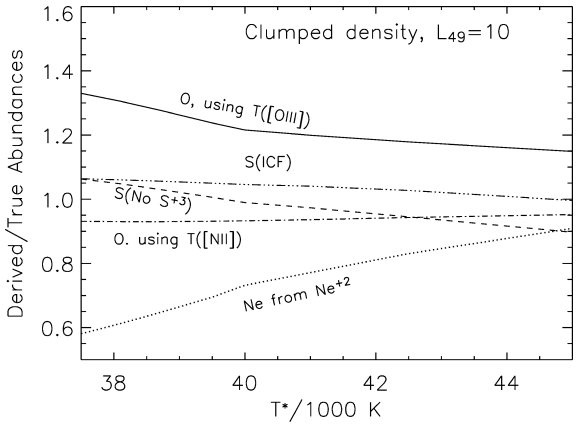

Figure 9. The total estimated global abundances of various elements. The elements and method of estimating its abundance are noted by the lines. For oxygen, 'using T([O III])' refers to the temperature used for O^+ and O^0, and similarly for 'using T([N II])'. T([O III]) is always used for O^{+2}. The S(ICF) is from an ionization correction factor to account for S^{+3} (see text).

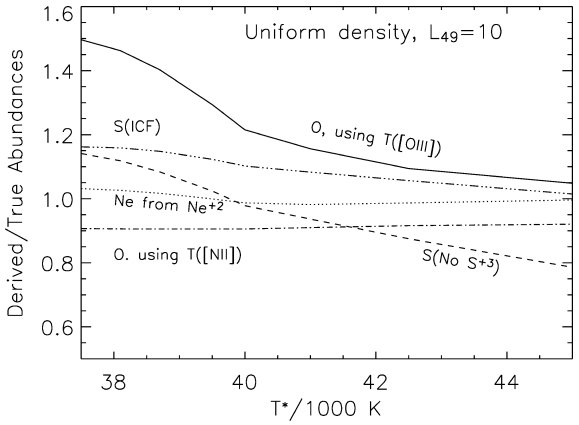

Figure 10. The total estimated global abundances of various elements. The elements and method of estimating its abundance are noted by the lines. For oxygen, 'using T([O III])' refers to the temperature used for O^+ and O^0, and similarly for 'using T([N II])'. T([O III]) is always used for O^{+2}. The S(ICF) is from an ionization correction factor to account for S^{+3}.

For clumped models, the global abundance of S^+ derived from T([O III]) (dashed lines in Fig. 7) is about twice the true abundances. The S^+ derived from T([N II]) is about 50 per cent too large.

Fig. 8 shows the trends of (S^{+2}/S). The bulk of sulfur is S^{+2}, but both S^+ and S^{+2} decrease with increasing T^*, showing the growing importance of S^{+3}.

The physically implausible assumption that all dielectronic recombination coefficients for S are zero leads to an appreciable shift of the abundances of S ions to the higher stages: from (S^+, S^{+2}, S^{+3}, S^{+4}) = (0.172, 0.762, 0.066, 5×10^{-5}) for $L_{49} = 10$, $T^* = 40$ kK clumped models to (0.115, 0.702, 0.182, 0.003) with no dielectronic recombination for S. Besides the obvious direct consequences for the S line strengths, the averaged electron temperature increases from 8751 to 8812 K because S^{+2} is a major coolant. However, the effects of geometry, T^* and L_{49} dominate the effects of the uncertainties in the dielectronic recombination coefficients of S.

3.5.5 Total abundances: O, Ne and S

Assuming that we have measures of both T([O III]) and T([N II]), how well can we estimate total elemental abundances from normally observed emission lines? Oxygen might provide the best case, because all of its ionization stages are observable. We include our estimates of O^0 in our discussion. In a real nebula it would be smaller than our prediction, while O^+ would be correspondingly larger.

Fig. 9 shows the estimated global abundances of O, Ne and S for clumped models, relative to the true abundance. The estimates for oxygen indicate which temperature is used to estimate O^+. T([O III]) is always used for O^{+2}. The estimate for Ne is derived from scaling the Ne^{+2} abundance by the model predictions of (Ne/Ne^{+2}). The line marked 'S(no S^{+3})' simply ignores that ion. The S(ICF) is based on an empirical ionization correction factor (ICF) to account for S^{+3} (Kwitter & Henry 2002). It relates $S/(S^+ + S^{+2})$ to (O/O^+):

$$S = (S^+ + S^{+2})\mathrm{ICF}; \quad (7)$$

$$\log(\mathrm{ICF}) = -0.17 + 0.18\beta - 0.11\beta^2 + 0.072\beta^3; \quad (8)$$

$$\beta = \log(O/O^+). \quad (9)$$

We see that the ICF provides an excellent estimate for the abundance of S.

Fig. 10 is similar to Fig. 9, except for uniform densities. For clumped models, there are compensating errors when we use T([N II]) for O^+ and T([O III]) for O^{+2}: the O^+ is too large, and the O^{+2} too small. For uniform models, both are only slightly too small. The net result is that the estimated abundance (dot-dashed lines in Figs 10 and 9) is found to be ∼310 ppM for all T^* and L_{49}, both uniform and clumped. Recall that in our models the true (O/H) = 330 ppM.

The importance of being able to use a suitable mean temperature [say, T([N II])] for low excitation ions is clear, especially for cool stars. If we are forced to use T([O III]) for O^+ as well as O^{+2}, both estimates are almost always too large (especially for O^+; see Fig. 5, dashed lines). They average about 400 ppM, and the worst (uniform, cool stars, $L_{49} = 100$) is a factor of 1.7 too large. The best case is for uniform geometry models excited by hot stars with $L_{49} = 100$. Its predicted oxygen is almost correct, but the corresponding clumped models predict 20 per cent more than the correct value. Clumping introduces appreciable uncertainties.

The plots of total abundances against T^* for other values of L_{49} are quite similar to those shown in Figs 9 and 10 for $L_{49} = 10$. For $L_{49} = 0.1$, the O using T([O III]) for O^+ (the solid line) is relatively flat at ∼120 per cent for both clumped and uniform models, an

improvement over the situation at $L_{49} = 10$. For $L_{49} = 1$, the curves are close to those in the figures. The total S without S^{+3} is also better for lower L_{49}, because the levels of high stages of ionization increase with L_{49}. For $L_{49} = 100$, the total S without S^{+3} varies from 110 per cent of the true at $T^* = 37.5$ kK to 83 per cent at 45 kK for clumped and 120 per cent to 66 per cent for uniform models.

4 REMARKS AND SUMMARY

The clumped ionization fractions differ significantly from uniform, and there are significant errors in estimating ionic abundances from emission-line fluxes. (He^+/H^+) is significantly increased for cool stars by clumping, and (He^0/He) is appreciable (2–3 per cent) for even very hot stars. Clumped models show less (O^{+2}/O) and (Ne^{+2}/Ne) than uniform for hot stars and more for cool. For clumped models, the abundances of both ions estimated by the standard methods using emission lines and the appropriate mean temperature, T([O III]), are only ∼70 per cent of the true abundances. For uniform models, the derived ionic abundances agree well with true. Real nebulae probably show the same phenomenon, and no improvement in spatial resolution will resolve it.

The strong effects of clumping on ionic abundances for a given stellar energy distribution (Section 3.5) make the determination of the properties of the exciting star from the nebular ionic ratios even more problematic than it is with smooth models. Another uncertainty is the presence of carbonaceous dust, with a strong absorption at ∼17 eV (Section 2), which makes the spectrum of the exciting star appear hotter because H-ionizing radiation is absorbed more readily than He-ionizing. Silicate dust makes little difference to H II regions because it has a low, almost wavelength-independent cross-section.

Real H II regions have irregular outer boundaries if they are bounded by ionization fronts. By means of models with clumped density distributions, we have investigated the effects of the complex shapes of the outer boundary on the analysis of ionic and elemental abundances. We feel that our models contain the elements of a basic physical effect that pertains to real H II regions in all of their geometrical complexities: their boundaries are also complex in shape, more so than our models.

We considered Kurucz (1994) stellar temperatures in the range 37.5–45 kK and ionizing photon luminosities of 10^{48}–10^{51} s^{-1}, all for an averaged density of 100 cm^{-3}. Of course, other models of stellar atmospheres have been proposed. The most important parameter of any of these is γ, the ratio of He-ionizing photons to H-ionizing. We considered γ in the range 0.57–2.4. Our results apply rather well for densities $n < 10^4$ cm^{-3} to objects with the same L_{49}/n as our models. With our limited spatial resolution, we found no regions truly shadowed from the central star. Clumping makes significant differences on the true abundances of ions of N, O, Ne and S, as well as those derived from emission lines plus measured nebular temperatures, T([O III]) and T([N II]). We considered two extreme limits of spatial resolution: either none, so that only the fluxes of the emission lines were used, or averaging the abundances as determined pixel-by-pixel over the face of the nebula. There were no major differences introduced by the two methods of averaging.

If T([N II]) is available for analysing the low stages of ionization, the overall abundances of O, Ne and S are reasonably accurate because of partially compensating errors. For cool stars (for which most Ne is Ne^+) in clumped models, (Ne/H) is badly estimated from [Ne III] optical lines. All of these elements are well estimated for uniform models. However, using T([O III]) for both low and high stages of ionization leads to overestimates of (O/H) of ∼40–60 per cent for both clumped and uniform models, for cool stars.

The underlying physical cause of the differences between clumped and uniform models is the flow of He recombination radiation from zones of high ionization of H that can be in physical proximity to regions near the outer edge of the nebula, with relatively large amounts of H^0. We discuss this effect in Section 3.1 and for each ion.

ACKNOWLEDGMENTS

JSM acknowledges support from a UK Particle Physics and Astronomy Research Council (PPARC) Short Term Visiting Fellowship to St Andrews, and KW from a PPARC Advanced Fellowship. Many of the models were produced with computing facilities granted to Professor Ellen Zweibel by the Graduate School of the University of Wisconsin-Madison. The comments of an anonymous referee improved the paper.

REFERENCES

Ackerman C. J., Carigi L., Nissen P. E., Pettini M., Asplund M., 2004, A&A, 414, 931
Ali B., Blum R. D., Bumgardner T. E., Cranmer S. R., Ferland G. J., Haefner R. I., Tiede G. P., 1991, PASP, 103, 1182
Asplund M., Grevesse N., Sauval A. J., Allende Prieto C., Blomme R., 2005, A&A, 431, 693
Elmegreen B., 1997, ApJ, 477, 196
Esteban C., Peimbert M., Torres-Peimbert S., García-Rojas J., Ruiz M. T., Rodríguez M., 1999a, ApJS, 120, 113
Esteban C., Peimbert M., Torres-Peimbert S., García-Rojas J., 1999b, RevMexA&A, 35, 65
Esteban C., Peimbert M., García-Rojas J., Ruiz M. T., Peimbert A., Rodríguez M., 2004, MNRAS, 355, 229
Ferland G. J., 1995, in Williams R., Livio M., eds, Space Telescope Science Institute Symposium 8, The Analysis of Emission Lines. Cambridge Univ. Press, Cambridge, p. 83
García-Rojas J., Esteban C., Peimbert M., Rodríguez M., Ruiz M. T., Peimbert A., 2004, ApJS, 153, 501
Holweger H., 2001, in Wimmer-Schweingruber R. F., ed., Proc. Joint SOHO/ACE Workshop, Vol. 598, Solar and Galactic Composition. Am. Inst. Phys., New York, p. 23
Howk J. C., Savage B. D., 1999, ApJ, 517, 746
Kurucz R. L., 1994, Solar Abundance Model Atmospheres, CD-Rom 19
Kwitter K. B., Henry R. B. C., 2001, ApJ, 562, 804
Lagache G., Haffner L. M., Reynolds R. J., Tufte S. L., 2000, A&A, 354, 247
Mathis J. S., Whitney B. A., Wood K., 2002, ApJ, 574, 812
O'Dell C. R., Peimbert M., Peimbert A., 2003, AJ, 125, 2590
Olive K. A., Skillman E. D., 2004, ApJ, 617, 29O
Osterbrock D. E., 1989, Astrophysics of Gaseous Nebulae and Active Galactic Nuclei. University Science Books, Mill Valley, CA
Pagel B. E. J., Tautvaišienė G., 1995, MNRAS, 276, 505
Peimbert M., Peimbert A., Ruiz M.-T., 2000, ApJ, 541, 688
Péquignot D. et al., 2001, in Ferland G., Savin D. W., eds, ASP Conf. Ser. Vol. 247, Spectroscopic Challenges of Photoionized Plasmas. Astron. Soc. Pac., San Francisco, p. 533
Savage B. D., Sembach K. R., 1996, ARA&A, 34, 279
Sellgren K., Tokunage A. T., Nakada Y., 1990, ApJ, 349, 120
Sofia U. J., Laroesch J. T., Meyer D., Cartledge S. I. B., 2004, ApJ, 605, 272
Tsamis Y. G., Barlow M. J., Liu X.-W., Danziger I. J., Storey P. J., 2003, MNRAS, 338, 687
Weingartner J. C., Draine B. T., 2001, ApJ, 548, 296
Wood K., Mathis J. S., Ercolano B., 2004, MNRAS, 348, 1337

This paper has been typeset from a TEX/LATEX file prepared by the author.